Manganite Memristive Devices: Recent Progress and Emerging Opportunities

A. Schulman

Facultad de Ciencias, Universidad de Salamanca, Salamanca, 37008, Spain

E-mail: schulman@usal.es

H. Huhtinen, and P Paturi

Department of Physics and Astronomy, University of Turku, Turku, FI-20014, Finland

Abstract.

Manganite-based memristive devices have emerged as promising candidates for next-generation non-volatile memory and neuromorphic computing applications, owing to their unique resistive switching behavior and tunable electronic properties. This review explores recent innovations in manganite-based memristive devices, with a focus on materials engineering, device architectures, and fabrication techniques. We delve into the underlying mechanisms governing resistive switching in manganite thin films, elucidating the intricate interplay of oxygen vacancies, charge carriers, and structural modifications.

This review underscores breakthroughs in harnessing manganite memristors for a range of applications, from high-density memory storage to neuromorphic computing platforms that mimic synaptic and neuronal functionalities. Additionally, we discuss the role of characterization techniques and the need for a unified benchmark for these devices. We provide insights into the challenges and opportunities associated with the co-integration of manganite-based memristive devices with more mature technologies, offering a roadmap for future research directions.

1. Introduction

Memristors, or memory resistors, have attracted significant attention in recent decades due to their unique functionality and potential applications [1–3]. These devices exhibit resistance switching behavior, altering their resistance based on the history of applied electrical stimulus. This inherent memory capability has opened avenues for high-density, low-power, non-volatile memory storage. Furthermore, the quasi-analog control of their conductance has unlocked their potential for use in neuromorphic computing systems [4–6], as they are capable of emulating both synaptic and neuronal functionalities. This has paved the way towards achieving fully memristive neuromorphic chips [7,8]. However, despite significant advances, the process technology and integration level for these type of devices are yet to meet the application requirements [9, 10].

The potential application of these devices in the exciting field of artificial intelligence and edge computing aroused significant interest and many recent review articles have focused on resistive switching on metal oxides [4, 11–14] and novel two-dimensional materials [15,16]. However, these are mainly focused on binary-type switching materials and devices, although lately there is an increasing interest in organic-inorganic halide materials [17]. This review article presents for the first time an overview of the progress made in memristive devices based on manganites as the main switching material.

Manganites, characterized by their perovskite crystal structure and diverse compositions within the general formula $R_{1-x}A_xMnO_3$ (where R represents a rare earth element, A denotes a divalent cation, and x represents the doping level), have emerged as a fascinating family of materials in the realm of solid-state physics and materials science [18, 19]. These compounds exhibit a rich spectrum of electronic and magnetic properties, stemming from the intricate interplay of charge, spin, and lattice degrees of freedom [20]. The phenomenon of colossal magnetoresistance (CMR), first observed in

certain manganite compositions, wherein a small change in an external magnetic field induces a significant change in electrical resistance, garnered widespread attention and prompted extensive research into manganite materials. Moreover, manganites possess intriguing phase transition behaviors, intricate spin configurations, and highly correlated electronic structures, offering a fertile ground for exploring novel functionalities.

In recent years, manganites have emerged as promising candidates for memristive applications, leveraging their unique properties to realize non-volatile memory storage, neuromorphic computing, and other advanced electronic functionalities [1,21,22]. This is mainly due to the inherent tunability of the fabricated devices combined with forming-free [23] and self-selecting switching behavior [24]. These memristive characteristics, combined with their low power consumption [4, 25], offer exciting prospects for the development of high-performance memristive devices with applications spanning from memory storage to brain-inspired computing architectures [26].

This review aims to provide a comprehensive overview of the recent innovations and future prospects in manganite-based memristive devices. We will explore the unique properties of manganites that render them suitable for memristive applications, discuss recent advancements in the design and fabrication of manganite-based memristive devices, and delve into the future prospects of these devices. In doing so, we aim to offer valuable insights for researchers and industry professionals in this rapidly evolving field, contributing to the ongoing efforts to realize the full potential of memristive devices for next-generation computing applications. The review is organized as follows: Section 2 discusses the fundamental principles of memristive devices and the unique properties of manganites; Section 3 explores recent advancements in manganite-based memristive devices; Section 4 discusses the future prospects of these devices; and Section 5 provides the concluding remarks.

2. Manganite-based Memristors: History and Working Principles

The concept of memristors, or memory resistors, was first introduced by Leon Chua in 1971 [27]. However, it wasn't until the late 20^{th} century that the first results of manganite-based memristors were reported thanks to the development of new fabrication processes that allowed obtaining high quality epitaxially grown films [28–30] . Having gained attention for their potential due to their colossal magnetoresistance (CMR) effect, where a small change in magnetic field can induce a large change in electrical resistance, memristor-based manganites generated big expectations due to the possibility of obtaining multifunctional devices where both magnetic and electrical properties are entangled [20]. Significant efforts were focused on understanding the underlying mechanisms of resistive switching in as well as optimizing device performance. Various fabrication techniques, including thin film deposition, nanostructuring, and interface engineering, were developed to tailor the properties of manganite memristors for specific applications such as non volatile memories, artificial synapses and neurons. In the table 1, we enumerate a selection of manganite-based memristor devices that have been

Table 1. Examples of manganite-based memristor devices and their key charactersitics

Switching material	Electrode material	Device type	$R_{on/off}$	Swtching speed	Endurance (cycles)	V_{th} (V)	Ref.
$Pr_{0.7}Ca_{0.3}MnO_3$	Au/Al	Planar	4	$\leq$ 100 μs	–	30	[35]
$Pr_{0.7}Ca_{0.3}MnO_3$	Ag/YBCO	Planar	4	$\leq$ 200 ns	–	30	[36]
$Pr_{0.7}Ca_{0.3}MnO_3$	Pt/YBCO	Planar	10^3	$\leq$ 200 ns	–	5	[28]
$Pr_{0.7}Ca_{0.3}MnO_3$	$SrRuO_3$/Ti	Capacitor	11	–	–	2	[29]
$Pr_{1-x}Ca_xMnO_3$	$SrRuO_3$/Ti	Capacitor	30	–	–	1.5	[37]
$Pr_{0.7}Ca_{0.3}MnO_3$	W/Pt	Capacitor	10^3	–	$>$ 200	1.5	[38]
$Pr_{0.7}Ca_{0.3}MnO_3$	Pt/W	Capacitor	10^3	$\leq$ 100 ns	$> 10^4$	2	[39]
$Pr_{0.6}Ca_{0.4}MnO_3$	Ag/Al	Planar	10^3	$\leq$ 100 μs	$> 10^5$	3	[23]
$Pr_{0.7}Ca_{0.3}MnO_3$	Ag/Al	Capacitor	10^2	$\leq$ 100 μs	$>$ 100	1.5	[40]
$La_{0.7}Ca_{0.3}MnO_3$	Al/Pt	Capacitor	15	$\leq$ 5 μs	$>$ 400	2	[41]
$La_{0.5}Ca_{0.5}MnO_3$	Ag/Pu	Planar	4	$\leq$ 5 μs	$>$ 100	2	[42]
$La_{0.67}Ca_{0.33}MnO_3$	n-Si/Ti	Capacitor	300	$\leq$ 5 ms	–	3	[43]
$La_{0.33}Ca_{0.67}MnO_3$	Pt/Ag	Capacitor	300	$\leq$ 1 ms	$> 5x10^4$	1	[44]
$La_{0.79}Sr_{0.21}MnO_3$	Pt/Ag	Capacitor	15	$\leq$ 200 ns	$> 10^3$	0.4	[45]
$La_{0.5}Sr_{0.5}MnO_3$	Au/Ti	Capacitor	30	–	–	4	[46]
$La_{0.79}Sr_{0.21}MnO_3$	Pt/Ag	Capacitor	10^5	–	$>$ 100	0.3	[47]
$La_{0.8}Sr_{0.2}MnO_3$	Ti/Pt	Planar	10	$\leq$ 60 ms	$>$ 30	4	[48]
$Nd_{0.7}Ca_{0.3}MnO_3$	Cu/Pt	Planar	10	–	–	40	[49]
$TbMnO_3$	Nb:$SrTiO_3$/Pt	Capacitor	10^4	$\leq$ 10 ms	100	2.5	[50]
$Gd_{1-x}Ca_xMnO_3$	Au/Al	Capacitor	100	$\leq$ 50 ms	10^4	3	[51]

reported along with the most relevant parameters. At first glance it may seem that manganite-based devices show less optimized qualities that other competing memristor materials such as Ta_2O_3 and HfO_2 [10, 31]. Nevertheless, manganite based devices are particularly well suited for analog control of the conductance making them ideal for neuromorphic applications [32, 33].

The ability to precisely control the formation and dissolution of oxygen vacancy chains through external voltage allows for very stable multi-level resistance states, which is a highly sought-after property for high density memory and analog computing. Additionally, manganite-based memristors tend to be forming-free devices, although they usually require some cycles to stabilize the resistive switching behaviour, it has the additional benefit to initialize the device after the fabrication process without the need to apply a larger voltage, which is a requirements for most simple oxide-based devices. Furthermore, in some cases, devices made from these materials are highly resistive and non-linear, which helps them be utilized as self-selector devices, simplifying the fabrication process of crossbar arrays. [34]

Table 1 reflects what is observed in the literature that $Pr_{0.7}Ca_{0.3}MnO_3$ is the most studied material. This is mostly due to historical reasons, as it was the first material to show the current switching of resistive states at low temperatures [52]. However, there is no indication that utilizing Pr offers any particular advantage over other rare earth materials like La and Gd. In fact, Gd-based devices showed better switching ratios than Pr-based ones as exemplified in Figure 1(a). As reported in [51], the improved

switching ratio relates to the work function difference between the manganite and the metal, in this case Al, as well as the bulk resistivity of the manganite. This is because the LRS of the device is related to the bulk resistivity while the HRS is linked to the Schottky barrier which is formed at the oxide/metal interface. The selection of appropriate manganite materials for resistive switching applications depends on several factors, including switching ratio, endurance, and scalability.

Another aspect that is worth pointing out is that most of the scope of reported devices was not the optimization of the memory properties but the understanding of the non-trivial phase transition behaviors, intricate spin configurations, and highly correlated electronic structures that characterize the manganite-based systems. For example, ref. [35] is a comparison of the effect on different systems, including manganites, cobaltites, titanates and nickelates. [36] and [28] utilize a superconducting electrode ($YBa_2Cu_3O_{7-\delta}$) both as a buffer layer and to investigate the proximity effect of the superconductivity and the CMR effect. Most of the reported works are focused on the optimization of different fabrication parameters such as composition [35, 37, 46, 51] and electrode material [29, 36, 48]; or the study of the electrical transport properties to gain understanding of the physical mechanism behind the resistive switching effect with the aim of providing with useful modeling tools [23, 28, 38, 41, 43, 44].

From the early reports on manganite-based memristors at the beginning of the century, it was already known that electrode materials play a key role in the performance of the devices. The choice of electrode materials plays a critical role in determining the performance and functionality of memristor devices. They serve as the interface between the memristive material and the external circuit, influencing factors such as electrical conductivity, adhesion, and compatibility with the memristive material. As such, the selection of electrode materials can have a great impact in the device characteristics. The devices functionalities are linked with at least two key parameters such as work function, which will relates with the electron injection, and its oxygen affinity, linked to the material oxidization [4, 21, 23, 29]. In figure 1(b) we can observe the effect of different electrodes, where this effect is observed only if at least one electrode is a reactive material (*e.g.* Ti, Al) that can form a barrier at the interface with the manganite. This barrier is the responsible of generating an electrochemical migration process that generates a zone near the electrode that affects the resistance of the junction [53] that can be tuned by the application of an electrical field. Therefore, is critically important to further understand the effect of the electrode material on all parameters of the device operation, including retention time, endurance, Set and Reset voltages, and $R_{on/Roff}$ ratios in order to improve on the desired properties of the devices.

The area of the electrode is frequently neglected in most reports and needs to be an important target for future device optimizations, if these materials are to compete with more advanced technologies like magnetic random access memories (MRAM) and phase change random access memories (PCRAM). It is commonly assumed that the electrode area has two different physical localizations depending on the switching type: the single filament model and the area-distributed switching. Typical switching scenarios can be

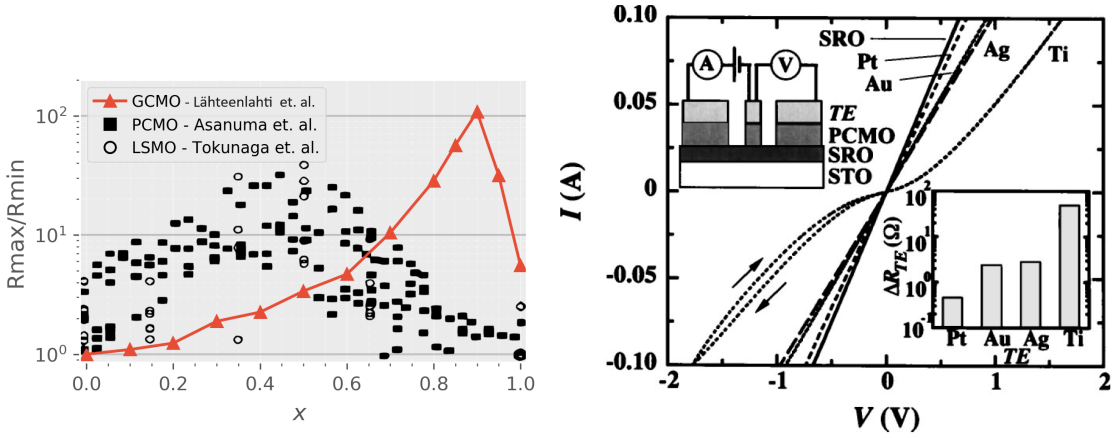

Figure 1. (a)Switching ratio over x for PCMO [37], GCMO [51], and LSMO [46]. from [51] with permission of the American Chemical Society (b) I–V characteristics of TE/$Pr_{0.7}Ca_{0.3}MnO_3$/$SrRuO_3$ layered structures with five different top electrodes ($SrRuO_3$, Pt, Au, Ag, Ti). The top-left inset shows a schematic of the measured device. The bottom-right inset presents the resistance for the five top electrodes utilized. From [29]. were Ohmic.

differentiated by measuring the area dependence of the low-resistance state as it should be completely independent if a single filament is formed. Although one can distinguish the type of switching by scaling the electrode area, the effect of the scaling itself has been seldom studied.

One notable milestone in manganite-based memristor research during this period was the elucidation of the role of oxygen vacancies and charge transport mechanisms in resistive switching phenomena [54, 55]. The family of manganite-based materials has some universal aspects of strongly correlated perovskites such as the doping-induced insulator-to-metal transition and spatial inhomogeneity (or phase separation) that occurs at the nanoscale and it is not linked to topological features [56]. Studies revealed that the migration of oxygen vacancies within the manganite lattice played a crucial role in modulating the resistance states of memristive devices. When an external voltage is applied to a manganite memristor, it induces a redistribution of oxygen vacancies, leading to localized changes in the oxygen stoichiometry [53, 57].In Figure 2, we present an example of the dead layer that is former at the interface between $Pr_{0.48}Ca_{0.52}MnO_3$ and Ti. Where Herpers *et. al.* [57] showed examined the device by Hard X-ray Photoelectron Spectroscopy (HAXPES) and found a clear correlation between the composition of the dead layer and the state of the device. This process, known as electrochemical metallization, involves the creation and dissolution of conductive filaments or paths within the manganite thin film. Typically, the as-prepared devices are in a high-resistance state, with a limited number of oxygen vacancies available for conduction. Manganites have a nontrivial spatial profile of the oxygen vacancy distribution which which tend to be accumulated near the electrodes. However, as the voltage is increased, oxygen vacancies migrate between the bulk of the manganite and anode/cathode,

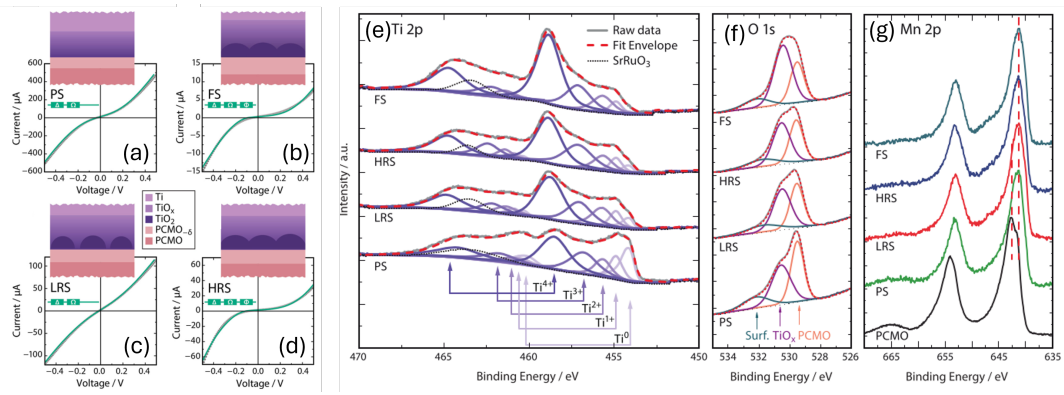

Figure 2. Electrical read-out data for the different resistance states for a $Ti/Pr_{0.48}Ca_{0.52}MnO_3/SrRuO_3$ device: (a) In the pristine state the Ti oxide layer is formed homogenously, (b) after electroforming a TiO_2 tunnel barrier is formed, (c) after a negative voltage sweep the tunnel barrier is bridged, (d) for the HRS the tunnel barrier is reformed. (e–g) Ti 2p/O 1s/Mn 2p XPS spectra collected on the four regions, sorted from low resistance (pristine) to high resistance (formed). Adapted from [57].

depending on the polarity of the applied voltage.

The cyclic migration of oxygen vacancies results in the formation of conductive filaments, effectively reducing the resistance of the device. This transition from a high-resistance state to a low-resistance state corresponds to the writing or programming of information in the memristor. Conversely, reversing the polarity of the applied voltage causes the dissolution of conductive filaments and restores the device to its original high-resistance state, effectively erasing or resetting the stored information. It is worth noting that the oxygen vacancies don't migrate from one electrode to the other, rather than the migration occurs in a confined area around each electrode es schematized in Figure 3. For example, we take the $Ti/Pr_{0.5}Ca_{0.5}MnO_3$ (PCMO) junction as a representative case [37], but we expect all manganite-based systems to behave in a similar manner. When a positive voltage bias was applied to the PCMO layer, the resistance state switches from the HRS to the LRS, as exemplified in Figure 3(d). In this case, positively charged oxygen vacancies are expected to migrate from the bulk zone into the dead layer composed of a-TiO_y. On the other hand, during the switching from the LRS to the HRS, oxygen vacancies are expected to migrate into the PCMO layer. It is therefore the number of oxygen vacancies in the vicinity of the interface what determines the state of the device. In the HRS, the highly oxygen-deficient manganite layer has a larger band gap and could act as an effective barrier to the electrical conduction, conversely, a small number of oxygen vacancies in the PCMO layer generates a smaller gap at the interface. This schematic representation of the switching is in agreement of what was observed by different spectroscopic technique as shown in Figure 2 and the interpretation for the modelling of the current-voltages results [54, 55].

Additionally, evidence of the movement of the oxygen vacancies during the switching events was reported for the manganite-based memristor $La_{0.67}Sr_{0.33}MnO_3$

deposited ontop of single crystal $SrTiO_3$ substrates [58]. Results for high resolution transmission microscopy (HRTEM), reveal a reversible migration of oxygen vacancies within the film, driven by combined effects of Joule heating and the applied electrical voltage. This led to a controlled switching between distinct resistance states. Figure 4 highlights the transformation between perovskite and brownmillerite phases due to oxygen vacancy ordering, further demonstrating the dynamic control of resistive states through voltage-induced oxygen vacancy manipulation. Other examples of direct observation of oxygen vacancies include the $La_{0.85}Sr_{0.15}MnO_3$ [59] and $Pr_{0.65}Ca_{0.35}MnO_3$ [60], showing that the effect indeed is expected to be universal for this family of devices.

Gaining the ability to precisely control the movement of oxygen vacancies will enable memristor devices to exhibit multi-state resistance switching, where multiple resistance levels can be achieved by varying the amplitude and duration of the applied voltage pulses [33]. Moreover, the nanoscale confinement and manipulation of oxygen vacancies within the manganite thin film enable memristors to operate with high speed, low power consumption, and excellent endurance [39]. In spite of great advancements in the last decade, efforts are still being developed to create a better control of the oxygen stoichiometry through controlled doping and annealing processes to achieve desired resistive switching characteristics.

3. Recent Advancements in Manganite-Based Memristive Devices

In recent years, there has been a notable surge in research directed towards leveraging manganite-based memristors (as well as memristors in general) for neuromorphic computing applications. Neuromorphic computing, inspired by the structure and functionality of biological nervous systems, aims to emulate the brain's efficient information processing capabilities using a massive parallelization scheme in order to develop the new generation of hardware based artificial neural networks. While two dimensional materials, binary oxides, and perovskite halides are gaining attention for their tunable band gaps and high charge mobility, manganite-based memristive devices offer distinct advantages in neuromorphic computing. The robust resistive switching characteristics of manganites, make them ideal for applications requiring stable, long-term performance. Manganite memristors, with their quasi analog control of the resistance and well as their low power consumption, offer a promising platform for implementing neuromorphic computing architectures.

For this, one fundamental aspect is the development of simulation methods that will enable to predict the behavior of the devices at large scales and how the will interface with the peripherical circuitry. The efforts in modelling and simulations can be divided into two groups, physical modelling and compact modelling. Different than the physical modelling that tries to explain the physical mechanism behind the memristive effect, compact models are models that are sufficiently simple to be incorporated in circuit simulators and are sufficiently accurate to make the outcome of the simulators useful to circuit designers. Although there are extremely useful, there is a fine line between

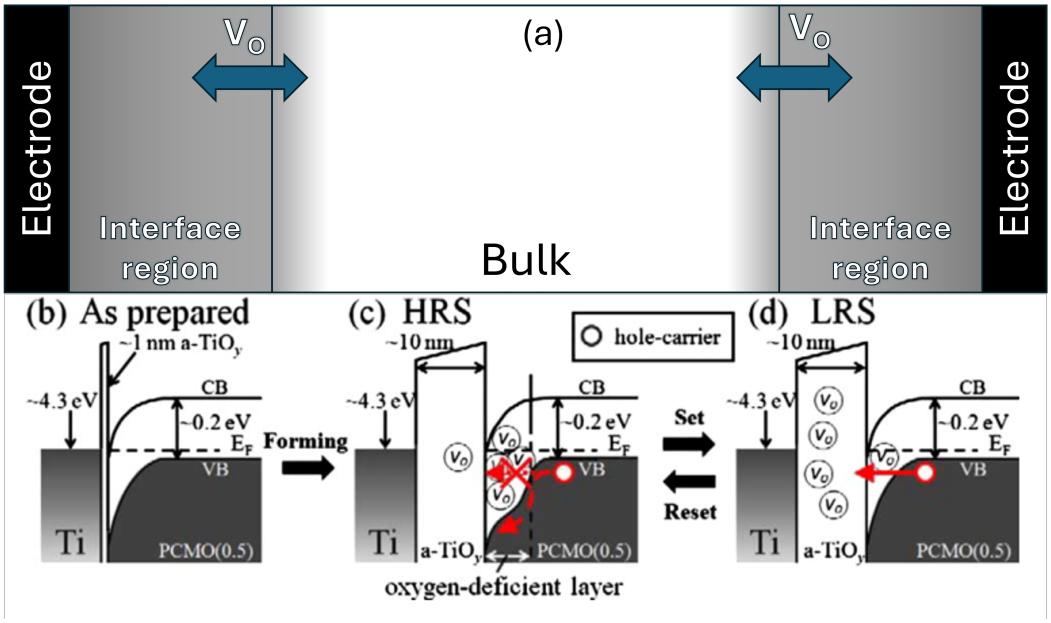

Figure 3. (a) Schematic of the working principle of a typical manganite-based memristor device. Upon fabrication a dead layer if formed due near the electrodes to the difference of work function between the metal and the oxides. Subsequently, upon cycling, the oxygen vacancies migrate reversible between this zone and a nearby region of the bulk where the effect is diluted due to being outside the influence area of the electrode induced band bending. The grey area represents the density of oxygen vacancies. (b-d) Possible band diagrams of Ti/$Pr_{0.5}Ca_{0.5}MnO_3$ (b) as-prepared, (c) in a high-resistance state, and (d) in a low-resistance state. In the HRS, the oxygen-deficient layer at the interface, having a larger band gap, acts as a barrier to hole-carrier conduction, created the darker shadowed region in (a). Adapted from [37]

model simplicity (*i.e.* usefulness) and accuracy make the compact modeling challenging research area for device physicists, modeling engineers and circuit designers [61].

Many groups have tackled the difficult task of creating a physically relevant model of the manganite-based devices [54, 55, 62–67]. All of the proposed models are based on a network of resistors that are linked to the movement of oxygen vacancies and the creation/dissolution of oxygen vacancy chains. Since the family of manganite-based materials has some universal aspects, most models are not material specific but rather are aimed at explain the conduction through the metal/oxide interface for the whole manganite family of materials. Let us explore the model developed by Rozenberg *et. al.* [55] in more detail. The model integrates three crucial aspects affecting manganite-based resistive switching phenomena: inhomogeneous conduction paths, the influence of defects, and the significance of interfaces. Firstly, it suggests that electric transport in the low resistive state is governed by one-dimensional paths formed under strong electric fields, implying a dominant conductive path within an insulating host. Secondly, the model incorporates the impact of defects, particularly oxygen vacancies, on resistivity, assuming a linear relation between oxygen vacancy concentration and local resistivity.

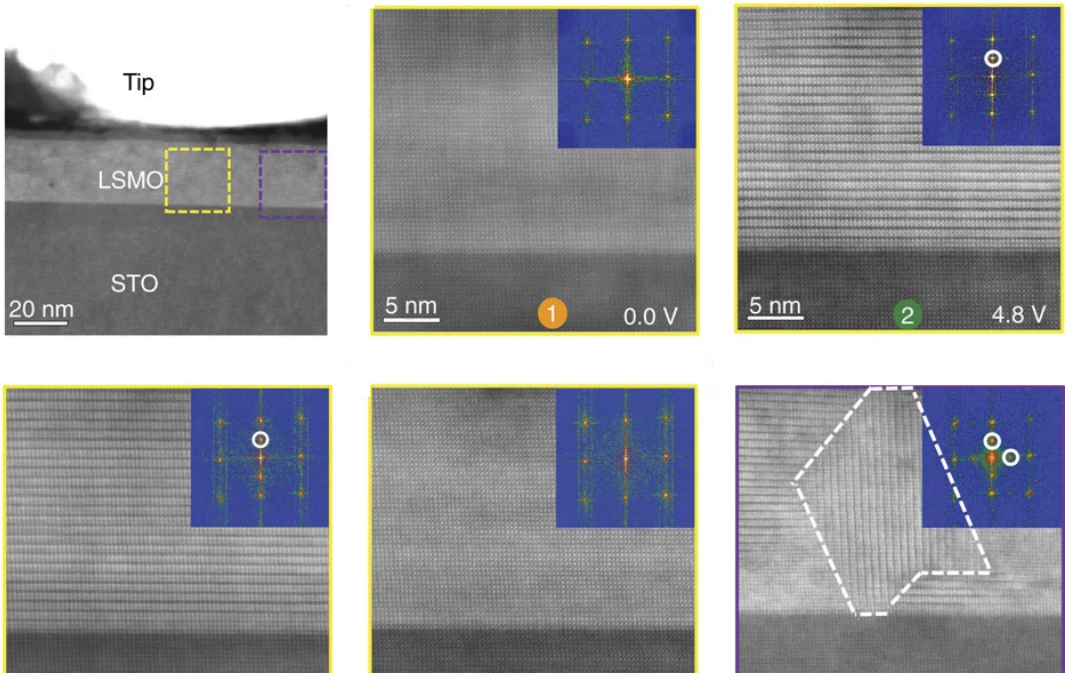

Figure 4. Cross-sectional STEM image of the contact between the metal tip and a $La_{0.67}Sr_{0.33}MnO_3$ film along with STEM HAADF images and their corresponding fast Fourier transform (FFT) patterns. They were taken at several stages of the bipolar resistive switching process. The STEM images indicate that switching to the high-resistance state by positive voltage pulses coincides with a uniform structural transition to the brownmillerite phase ((1)→(2)), whereas the low-resistance perovskite structure is re-established by negative voltage pulses ((3)→(4)). From [58]

Lastly, it emphasizes the importance of interfaces, suggesting that resistive switching primarily occurs in regions near metallic electrodes. The model, depicted schematically in Figure 5, consists of a conductive channel within an insulating dielectric, represented as a one-dimensional resistive network. Numerical simulations involve applying voltage protocols, computing current, updating oxygen vacancy concentrations, and iteratively computing current under the applied voltage, considering the impact of oxygen vacancy transfers between neighboring domains.

The results of the simulations are presented in the form of hysteresis switching loops, which can be observed along with experimental measurements in Figure 5 (c-e). After a couple of forming cycles, the device converges to a stable hysteresis loop termed "table with legs". This distinctive loop is successfully replicated in experimental studies in both manganite and cuprate samples, this highlights the generalization potential of the model. The qualitative agreement between the model's prediction and experimental hysteresis loops underscores the model's ability to capture non-trivial features by having the capacity to elucidate underlying mechanisms governing resistive switching phenomena in oxide materials, particularly the importance of the region near the electrode and the

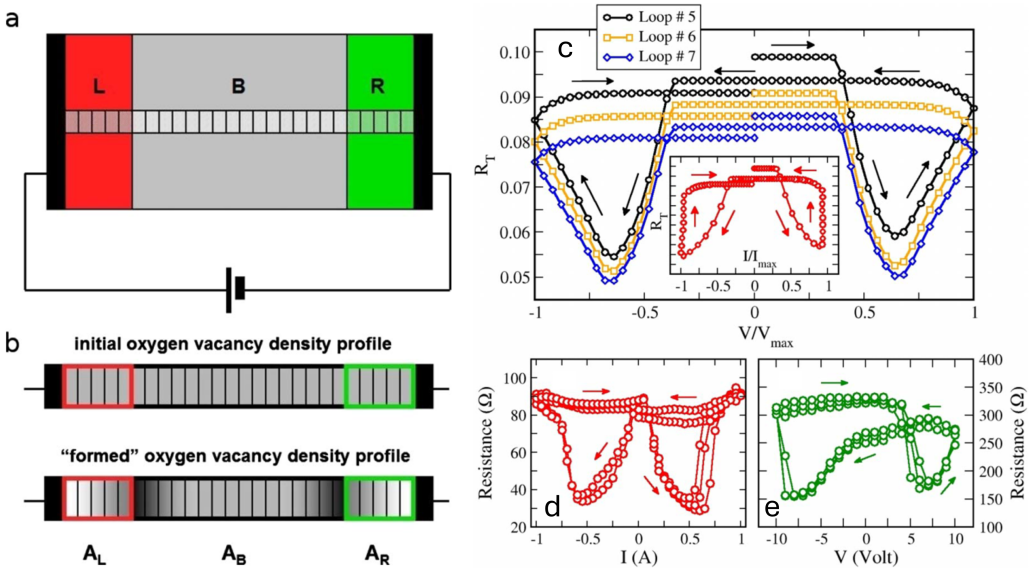

Figure 5. (a) Schematic model with a single conductive channel within the dielectric. The three regions L, R, and B correspond to the two high resistance interfaces and the more conductive central bulk, respectively. The small boxes indicate the domains. (b) Detailed scheme of the conductive path. The grayscale qualitatively depicts the variation in the oxygen vacancy concentration through the channel where darker corresponds to a higher concentration. (c) Resistive hysteresis loop for the voltage cycles obtained from the model. Experimental hysteresis loops measured in (d) $Ag/La_{0.325}Pr_{0.300}Ca_{0.375}MnO_3/Au$ and (c) $Ag/YBa_2Cu_3O_{7-\delta}/Pt$. Adapted from [55]

dynamics of the oxygen vacancies with the electrical field.

Moving beyond physical models, Let's shift focus to compact modeling, especially as this technology advances up the Technology Readiness Level (TRL) scale. There is a growing interest in co-integrating memristors with other technologies, making it essential to have models that can be seamlessly integrated into circuit simulators, to unleash the full potential of this technology. Unlike physical mechanisms, there isn't a unified approach to creating compact models. The choice of programming language, such as Verilog, LTSPICE, and others, significantly influences the utility of the model. Moreover, the balance between faithfulness to the actual device and robustness, as well as computing speed, becomes a crucial consideration. Ensuring accurate representation of device behavior while maintaining computational efficiency is paramount for practical implementation. Several models have been proposed with a varying degree of fidelity and efficiency [34, 68–76].

One model that is worth mentioned is the so-called memdiode model developed by Miranda *et. al.* [44, 76], written in the LTspice language. The main advantage is the simplified approach due to the elimination of the time integration step in favor of the use of the so-called hysteron or memory map. However, even though a time module can be added to the base model at a computation cost [34], the base model is in essence a quasi-static approach in the sense that the memory state of the device does not change

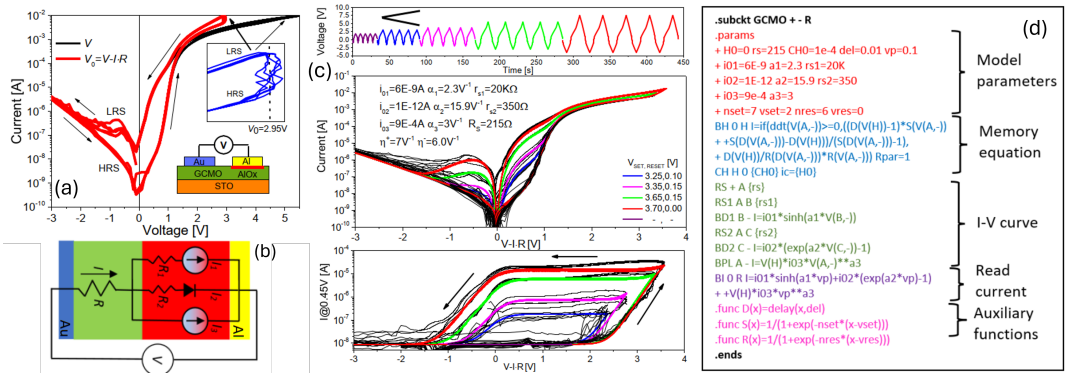

Figure 6. a) Experimental current-voltage curve for a Al/$Gd_{0.85}Ca_{0.15}MnO_3$/Au device. top inset: Detail of the current increase at the voltage threshold. Bottom inset: Structure of the investigated devices. b) Equivalent circuit model. (c) Ability of the model (color) to simulate the experimental multilevel results (black) as a function of the applied bias. (d) Full model script for LTSPICE. Adapted from [76].

unless a hard threshold condition is met. It is important to note that can be used for arbitrary input signals, but the memory state is unable to evolve in the subthreshold regime. An example of this model was reported in [76] where the multilevel conduction of a Al/$Gd_{0.85}Ca_{0.15}MnO_3$/Au is parametrized and modeled with great precision. Figure 6 shows the equivalent circuit utilized to parameterise the device along the results of the model. A critical requirement for analog memristors is to account for intermediate states, which allow for a fine tuning required in synaptic applications in neuromorphic circuits. This is experimentally presented in Figure 6(c), which is accurately simulated by the memdiode model. The model itself is written as a module of LTSPICE and can be found in its entirety in Figure 6(d). It is structured into five modular sections, each of which can be adjusted to accommodate specific transport properties and transition dynamics of each device. The subcircuit has three physical terminals for the device (+ and -), with R providing the read current. The initial section defines model parameters such as the initial memory state, the capacitor used for memory storage, the delay parameter, and the read voltage. The second section implements a discretized memory equation using a behavioral voltage-controlled current source, with the delay function facilitating information retrieval. The third section describes the I-V port using the hysteron equations, with the voltage node modulating the power-law soft-breakdown current component. An optional fourth section calculates the read current at any given voltage pulse, either by duplicating the I-V port for a fixed voltage or by neglecting the series resistances. Finally, the last section defines delay and ridge functions.

As one of the main characteristics of manganite-based devices is the quasi-analog conductance, they are particularly well suited as artificial synapses [31]. Synapses are crucial components of biological neural networks, facilitating the transmission of signals between neurons and enabling learning and memory functionalities. Recent research efforts have focused on optimizing the synaptic behavior of manganite memristors,

including achieving long-term potentiation and depression (LTP/LTD), short-term potentiation and depression (STP/STD), and spiking-time dependent plasticity (STDP) through voltage and current stimuli. Due to its nonvolatile nature, the synaptic weight of the devices can theoretically be regulated and maintain indefinitely depending on the history of the applied external stimuli. This feature is quite analogous to the activity-dependent regulation of synaptic plasticity in biology. Departing from standard memory characterizations such as retention or on/off resistance ratio, new parameters need to be taken into account to asses the performance of a synaptic device, such as multi-level states, linearity and symmetry. As one of the key learning mechanisms, The STDP is a kind of Hebbian learning rule [77] for which the synaptic strength increase or decrease exponentially depending on the delay time between the pre- and post-synaptic pulses. STDP can be achieved using memristive devices by purposely designing pulse width, the number of pulses, and pulse voltage amplitude. Different implementations of STDP have been reported in manganite memristors [78–84]. An example of implementation for different manganite material are shown in Figure 7. In the Figure, we can observe that regardless of the material, they all show very similar curves with the main difference being the parameters utilized (timings and voltages). Continuing the advancement of manganite-based devices as artificial synapses entails meticulous steps toward achieving enhanced performance and functionality within neuromorphic computing architectures. One pivotal aspect is the judicious selection and refinement of algorithms tailored to the specific characteristics of manganite memristors. Such algorithms necessitate thorough consideration of device variability, noise, and nonlinearity to optimize performance effectively. For this, recent reports that focused this efforts on manganite-based memristors have shown significant progress in their application for neuromorphic computing and high-density memory storage. For instance, Quiñonez et al. [85] explored the effect of potentiation-depression curves, which is crucial for the convergence of physical perceptrons used in neuromorphic systems. Their findings highlight the importance of understanding the dynamic behavior of these devices to optimize their performance in artificial neural networks. Additionally, Saraswat et al. [86] analyzed the neuromorphic potential of these devices, further demonstrating their applicability in neural networks and learning systems. Yeon et al. [87] showcased the effect of oxygen vacancy on the conduction modulation linearity in $Pr_{0.67}Ca_{0.33}MnO_3$ memristors, underscoring the importance of the linearity of the conductance chance in the accuracy of the neural network.

All these work highlight the importance of advancing beyond individual synapses requires the development of larger networks comprising interconnected manganite-based artificial synapses. Scaling up to larger networks enables the emulation of complex neural architectures and computational tasks. While some efftors have been reported in the fabrication of crossbar arrays [39,40,68,88], there still open challenges such as addressing interconnectivity, synchronization, and scalability within the network design. Successful development of larger networks will enable the exploration of advanced functionalities, including pattern recognition, learning, and inference, within the realm of neuromorphic

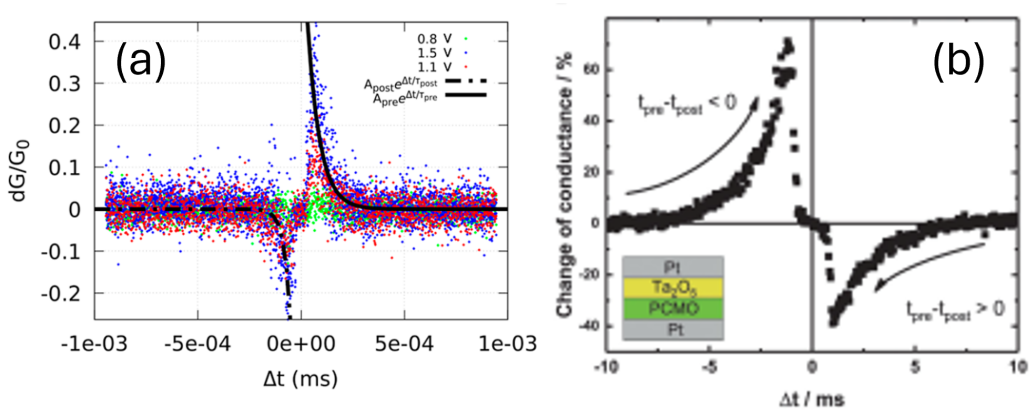

Figure 7. Relative change of conductance for different time delays between the pre- and post-synaptic pulse during STDP measurement for the three different devices. (a) $Gd_{0.85}Ca_{0.15}MnO_3$ from [84], (b) $Pr_{0.67}Ca_{0.33}MnO_3$ from [83].

systems.

4. Future Prospects

The future of manganite-based memristive devices is still uncertain, with opportunities for, further innovation and integration into a wide range of applications but with the drawbacks that they are difficult materials to produce at large scale and process with standard semiconducting techniques. As researchers continue to explore the capabilities of manganite memristors, several key areas emerge as focal points for future development and advancement.

One area of future prospects lies in the optimization of the fabrication of manganite memristors for a seamless co-integration with complementary metal oxide semiconductor (CMOS) technologies. The exploration of novel fabrication methods, materials and device architectures holds promise for enhancing the performance and functionality of manganite memristors. Researchers are investigating alternative manganite compositions, heterostructures, and nanostructures to achieve superior memristive properties, including faster switching speeds, higher endurance, and multi-state resistance modulation. Furthermore, advancements in fabrication techniques, such as bottom-up assembly and 3D printing, offer opportunities for scalable and cost-effective production of manganite memristor arrays for practical applications.

Furthermore, the integration of manganite memristors with other emerging technologies, such as artificial magnetic RRAM and Si-bassed artificial neurons, presents intriguing possibilities for future interdisciplinary research and development. By combining the unique functionalities of manganite materials with complementary technologies, researchers could help to address pressing societal challenges in diverse fields, including beyond Von Neumann computing, healthcare, energy, and environmental monitoring.

5. Concluding Remarks

In conclusion, the comprehensive exploration of manganite-based memristive devices presented in this review underscores their significance as key components in the evolving landscape of electronic and cognitive computing. From their historical roots to recent advancements and future prospects, manganite memristors have demonstrated immense potential for revolutionizing various applications, including non-volatile memory storage, neuromorphic computing, and artificial intelligence.

Throughout this review, we have highlighted the unique properties of manganite materials and their role in enabling the resistive switching behavior observed in memristive devices. The dynamic interplay of oxygen vacancie and structural modifications within the manganite lattice governs the functionality of memristors, offering opportunities for tailored device performance and functionality. We also discussed the importance of simulations an modelling as well as different ways to implement this results. From the optimization of materials and device architectures to the integration with complementary technologies, researchers continue to push the boundaries of manganite memristors towards higher TRL research and real societal impact.

In closing, this review aims to inspire continued exploration and collaboration in the field of manganite-based memristive devices, contributing to the ongoing efforts to realize the transformative impact of memristors within the growing field of next-generation computing.

Acknowledgments

This project has received funding from the European Union's Horizon 2020 research and innovation programme under the Marie Skłodowska-Curie grant agreement No 101034371 as well as the Academy of Finland project 352802. The authors also acknowledge the Jenny and Antti Wihuri Foundation for financial support.

References

[1] Waser R and Aono M 2007 *Nat. Mater.* **6** 833–840
[2] Ielmini D and Waser R (eds) 2016 *Resistive switching* (Weinheim, Germany: Wiley-VCH Verlag)
[3] Suñé J 2020 *Memristors for neuromorphic circuits and artificial Intelligence applications* (Mdpi AG)
[4] Chen S and Valov I 2022 *Adv. Mater.* **34** e2105022
[5] Yang J J, Strukov D B and Stewart D R 2013 *Nat. Nanotechnol.* **8** 13–24
[6] Zhang Y, Wang Z, Zhu J, Yang Y, Rao M, Song W, Zhuo Y, Zhang X, Cui M, Shen L, Huang R and Joshua Yang J 2020 *Appl. Phys. Rev.* **7** 011308
[7] Yao P, Wu H, Gao B, Tang J, Zhang Q, Zhang W, Yang J J and Qian H 2020 *Nature* **577** 641–646
[8] Wang Z, Joshi S, Savel'ev S, Song W, Midya R, Li Y, Rao M, Yan P, Asapu S, Zhuo Y, Jiang H, Lin P, Li C, Yoon J H, Upadhyay N K, Zhang J, Hu M, Strachan J P, Barnell M, Wu Q, Wu H, Williams R S, Xia Q and Yang J J 2018 *Nat. Electron.* **1** 137–145
[9] del Valle J, Ramírez J G, Rozenberg M J and Schuller I K 2018 *J. Appl. Phys.* **124** 211101

[10] Xia Q and Yang J J 2019 *Nat. Mater.* **18** 309–323
[11] Pan F, Gao S, Chen C, Song C and Zeng F 2014 *Mater. Sci. Eng. R Rep.* **83** 1–59
[12] Bagdzevicius S, Maas K, Boudard M and Burriel M 2017 *J. Electroceram.* **39** 157–184
[13] Dittmann R, Menzel S and Waser R 2021 *Adv. Phys.* **70** 155–349
[14] Zhang G, Qin J, Zhang Y, Gong G, Xiong Z Y, Ma X, Lv Z, Zhou Y and Han S T 2023 *Adv. Funct. Mater.* **33**
[15] Zhang L, Xu K and Wei F 2023 *J. Mater. Sci.* **58** 2087–2110
[16] Lanza M, Hui F, Wen C and Ferrari A C 2023 *Adv. Mater.* **35** e2205402
[17] Qammar M, Zou B and Halpert J E 2023 *J. Semicond.* **44** 091604
[18] Dagotto E, Hotta T and Moreo A 2001 *Phys. Rep.* **344** 1–153
[19] Coey J M D, Viret M and von Molnár S 1999 *Adv. Phys.* **48** 167–293
[20] Salamon M B and Jaime M 2001 *Rev. Mod. Phys.* **73** 583–628
[21] Sawa A 2008 *Mater. Today (Kidlington)* **11** 28–36
[22] Waser R, Dittmann R, Staikov G and Szot K 2009 *Adv. Mater.* **21** 2632–2663
[23] Lähteenlahti V, Schulman A, Huhtinen H and Paturi P 2019 *J. Alloys Compd.* **786** 84–90
[24] Lashkare S, Panwar N, Kumbhare P, Das B and Ganguly U 2017 *IEEE Electron Device Lett.* **38** 1212–1215
[25] Liu X, Biju K P, Bourim E M, Park S, Lee W, Shin J and Hwang H 2010 *Solid State Commun.* **150** 2231–2235
[26] Li Y, Wang Z, Midya R, Xia Q and Yang J J 2018 *J. Phys. D Appl. Phys.* **51** 503002
[27] Chua L 1971 *IEEE Trans. Circuit Theory* **18** 507–519
[28] Liu S Q, Wu N J and Ignatiev A 2000 *Appl. Phys. Lett.* **76** 2749–2751
[29] Sawa A, Fujii T, Kawasaki M and Tokura Y 2004 *Appl. Phys. Lett.* **85** 4073–4075
[30] Tsui S, Baikalov A, Cmaidalka J, Sun Y Y, Wang Y Q, Xue Y Y, Chu C W, Chen L and Jacobson A J 2004 *Appl. Phys. Lett.* **85** 317–319
[31] Zhu J, Zhang T, Yang Y and Huang R 2020 *Appl. Phys. Rev.* **7** 011312
[32] Gomez-Marlasca F, Ghenzi N, Stoliar P, Sánchez M J, Rozenberg M J, Leyva G and Levy P 2011 *Appl. Phys. Lett.* **98** 123502
[33] Stoliar P, Levy P, Sanchez M J, Leyva A G, Albornoz C A, Gomez-Marlasca F, Zanini A, Toro Salazar C, Ghenzi N and Rozenberg M J 2014 *IEEE Trans. Circuits Syst. II Express Briefs* **61** 21–25
[34] Aguirre F L, Suñé J and Miranda E 2022 *Micromachines (Basel)* **13** 330
[35] Hamaguchi M, Aoyama K, Asanuma S, Uesu Y and Katsufuji T 2006 *Appl. Phys. Lett.* **88** 142508
[36] Baikalov A, Wang Y Q, Shen B, Lorenz B, Tsui S, Sun Y Y, Xue Y Y and Chu C W 2003 *Appl. Phys. Lett.* **83** 957–959
[37] Asanuma S, Akoh H, Yamada H and Sawa A 2009 *Phys. Rev. B Condens. Matter Mater. Phys.* **80**
[38] Liu X, Biju K P, Bourim E M, Park S, Lee W, Shin J and Hwang H 2010 *Solid State Commun.* **150** 2231–2235
[39] Kumbhare P, Chakraborty I, Khanna A and Ganguly U 2017 *IEEE Trans. Electron Devices* **64** 3967–3970
[40] Park S, Jung S, Siddik M, Jo M, Lee J, Park J, Lee W, Kim S, Sadaf S M, Liu X and Hwang H 2011 *Phys. Status Solidi Rapid Res. Lett.* **5** 409–411
[41] Yang R, Li X M, Yu W D, Liu X J, Cao X, Wang Q and Chen L D 2009 *Electrochem. Solid State Letters* **12** H281
[42] Wang Z H, Yang Y, Gu L, Habermeier H U, Yu R C, Zhao T Y, Sun J R and Shen B G 2012 *Nanotechnology* **23** 265202
[43] Rubi D, Tesler F, Alposta I, Kalstein A, Ghenzi N, Gomez-Marlasca F, Rozenberg M and Levy P 2013 *Appl. Phys. Lett.* **103** 163506
[44] Miranda E, Román Acevedo W, Rubi D, Lüders U, Granell P, Suñé J and Levy P 2017 *J. Appl. Phys.* **121** 205302

[45] Liu D, Cheng H, Zhu X, Wang G and Wang N 2013 *ACS Appl. Mater. Interfaces* **5** 11258–11264
[46] Tokunaga Y, Kaneko Y, He J P, Arima T, Sawa A, Fujii T, Kawasaki M and Tokura Y 2006 *Appl. Phys. Lett.* **88** 223507
[47] Liu D, Wang N, Wang G, Shao Z, Zhu X, Zhang C and Cheng H 2013 *Appl. Phys. Lett.* **102** 134105
[48] Moncasi C, Lefèvre G, Villeger Q, Rapenne L, Roussel H, Bsiesy A, Jiménez C and Burriel M 2022 *Adv. Mater. Interfaces* **9** 2200498
[49] Hsu D, Lin J G, Wu W F, Wu C T and Chen C H 2007 *IEEE Trans. Magn.* **43** 3067–3069
[50] Cui Y, Peng H, Wu S, Wang R and Wu T 2013 *ACS Appl. Mater. Interfaces* **5** 1213–1217
[51] Lähteenlahti V, Schulman A, Beiranvand A, Huhtinen H and Paturi P 2021 *ACS Appl. Mater. Interfaces* **13** 18365–18371
[52] Asamitsu A, Tomioka Y, Kuwahara H and Tokura Y 1997 *Nature* **388** 50–52
[53] Yamamoto T, Yasuhara R, Ohkubo I, Kumigashira H and Oshima M 2011 *J. Appl. Phys.* **110** 053707
[54] Rozenberg M J, Inoue I H and Sánchez M J 2004 *Phys. Rev. Lett.* **92** 178302
[55] Rozenberg M J, Sánchez M J, Weht R, Acha C, Gomez-Marlasca F and Levy P 2010 *Phys. Rev. B Condens. Matter Mater. Phys.* **81**
[56] Becker T, Streng C, Luo Y, Moshnyaga V, Damaschke B, Shannon N and Samwer K 2002 *Phys. Rev. Lett.* **89** 237203
[57] Herpers A, Lenser C, Park C, Offi F, Borgatti F, Panaccione G, Menzel S, Waser R and Dittmann R 2014 *Adv. Mater.* **26** 2730–2735
[58] Yao L, Inkinen S and van Dijken S 2017 *Nat. Commun.* **8** 14544
[59] Chowdhury P M and Raychaudhuri A K 2021 *Mater. Res. Bull.* **137** 111160
[60] Kramer T, Mierwaldt D, Scherff M, Kanbach M and Jooss C 2018 *Ultramicroscopy* **184** 61–70
[61] Gildenblat G (ed) 2010 *Compact Modeling* (Dordrecht, Netherlands: Springer)
[62] Zhirnov V V, Meade R, Cavin R K and Sandhu G 2011 *Nanotechnology* **22** 254027
[63] Guan X, Yu S and Wong H S P 2012 *IEEE Trans. Electron Devices* **59** 1172–1182
[64] Kamiya K, Young Yang M, Park S G, Magyari-Köpe B, Nishi Y, Niwa M and Shiraishi K 2012 *Appl. Phys. Lett.* **100** 073502
[65] Niraula D and Karpov V 2018 *J. Appl. Phys.* **124** 174502
[66] Noma T, Taguchi D, Manaka T and Iwamoto M 2018 *J. Appl. Phys.* **124** 175501
[67] Koushan F S and Kobayashi N P 2020 *J. Appl. Phys.* **128** 165302
[68] Aguirre F L, Pazos S M, Palumbo F, Suñé J and Miranda E 2021 *Front. Phys.* **9**
[69] Coulié K, Aziza H and Rahajandraibe W 2023 *J. Electron. Test.* **39** 275–288
[70] Jimenez-Leon J, Sarmiento-Reyes L A and Rosales-Quintero P 2022 *IEEE Trans. Comput.-aided Des. Integr. Circuits Syst.* **41** 4851–4861
[71] Kumar S and Das D M 2021 Python-LTspice co-simulation to train neural networks with memristive synapses to learn logic gate operations *2021 IEEE International Symposium on Smart Electronic Systems (iSES)* (IEEE)
[72] Saludes-Tapia M, Gonzalez M B, Campabadal F, Suñé J and Miranda E 2021 *Solid State Electron.* **185** 108083
[73] Soni K and Sahoo S 2022 A review on different memristor modeling and applications *2022 International Mobile and Embedded Technology Conference (MECON)* (IEEE)
[74] Zeumault A, Alam S, Omar Faruk M and Aziz A 2022 *J. Appl. Phys.* **131** 124502
[75] Zhang Y, He G, Tang K T, Li Y and Wang G 2023 *IEEE Trans. Comput.-aided Des. Integr. Circuits Syst.* **42** 834–846
[76] Miranda E, Lahteenlahti V, Huhtinen H, Schulman A and Paturi P 2022 *IEEE Trans. Nanotechnol.* **21** 285–288
[77] Hebb D (ed) 1949 *The Organization Of Behavior* (New Jersey, United Statesy: John Wiley Sons)
[78] Zamarreño-Ramos C, Camuñas-Mesa L A, Pérez-Carrasco J A, Masquelier T, Serrano-Gotarredona T and Linares-Barranco B 2011 *Front. Neurosci.* **5** 26

[79] Sheri A M, Hwang H, Jeon M and Lee B G 2014 *IEEE Trans. Ind. Electron.* **61** 2933–2941
[80] Jang J W, Park S, Burr G W, Hwang H and Jeong Y H 2015 *IEEE Electron Device Lett.* **36** 457–459
[81] Park S, Chu M, Kim J, Noh J, Jeon M, Hun Lee B, Hwang H, Lee B and Lee B G 2015 *Sci. Rep.* **5** 10123
[82] Lashkare S, Panwar N, Kumbhare P, Das B and Ganguly U 2017 *IEEE Electron Device Lett.* **38** 1212–1215
[83] Gutsche A, Siegel S, Zhang J, Hambsch S and Dittmann R 2021 *Front. Neurosci.* **15** 661261
[84] Hynnä T, Schulman A, Lähteenlahti V, Huhtinen H and Paturi P 2024 *ACS Appl. Electron. Mater.* **6** 292–298
[85] Quiñonez W, Sánchez M J and Rubi D 2023 *Phys. Scr.* **98** 095917
[86] Saraswat V and Ganguly U 2022 *Neuromorph. Comput. Eng.* **2** 014001
[87] Pyo Y, Woo J U, Hwang H G, Nahm S and Jeong J 2021 *Nanomaterials (Basel)* **11** 2684
[88] Hong E, Jeon S, Kim N, Kim H W, Kang H, Moon K and Woo J 2023 *AIP Adv.* **13** 015318